Sukhvir Singh[1], Niranjan Bhowmick[1], Anand Vaz[2]
[1] Dr. B. R. Ambedkar National Institute of Technology, Department of Textile Technology, Jalandhar-144011, Punjab, India
[2] Dr. B. R. Ambedkar National Institute of Technology, Department of Mechanical Engineering, Jalandhar-144011, Punjab, India

Theoretical Modelling of Can-spring Mechanism Using Bond Graph

Teoretično modeliranje mehanizma vzmeti v loncu z uporabo veznega grafa

Original scientific article/*Izvirni znanstveni članek*
Received/*Prispelo* 11-2019 • Accepted/*Sprejeto* 2-2020

Abstract

Helical compression springs are extensively used for the combed cotton sliver handling system in spinning preparatory sections in the textile industry. Storage can-spring stiffness decreases with time due to prolonged fatigue loading. It has been found that older storage can-springs of reduced spring stiffness deform non-uniformly during combed sliver deposition and withdrawal. In order to produce consistent quality of an intermediate delicate product like combed sliver, sliver stresses should be monitored meticulously at the time of sliver deposition and withdrawal from storage cans. The present research is an attempt to study the dynamics of the can-spring mechanism used for sliver storage through the bond graph approach. The paper records the first stage of the work, which is concerned with establishing the relationship between spring stiffness and sliver forces. Bond graph modelling of the can-spring mechanism is one of thebest-suited approaches to study the present research problem due to its characteristic features.
Keywords: bond graph, combed cotton sliver, can-spring stiffness, storage can

Izvleček

Vijačne tlačne vzmeti se pogosto uporabljajo v tekstilni industriji pri rokovanju s česanim bombažnim pramenom pri pripravi na predenje. Togost vzmeti v loncih se lahko ob dolgotrajnih obremenitvah sčasoma zmanjša zaradi utrujenosti. Ugotovljeno je bilo, da se starejše vzmeti z zmanjšano togostjo med odlaganjem česanega pramena v lonce in vlečenjem iz loncev neenakomerno deformirajo. Da bi dosegli stalno kakovost tako zelo občutljivega polizdelka, kot je česani pramen, je potrebno skrbno nadzirati napetost pramena v času odlaganja v lonec in vlečenja pramena iz lonca. Raziskava predstavlja primer uporabe veznega grafa za študij dinamike mehanizma vzmeti, ki se uporabljajo v loncih za shranjevanje pramena. V članku je predstavljena prva faza raziskav, tj. vzpostavljanje odvisnosti med togostjo vzmeti in silami, ki delujejo na pramen. Modeliranje veznega grafa za mehanizem vzmeti v loncu je zaradi njegovih značilnosti eden najprimernejših pristopov k preučevanju predstavljenega raziskovalnega problema.
Ključne besede: vezni graf, česan bombažni pramen, togost vzmeti v loncu, lonec

1 Introduction

In the process of making short-staple yarn from fibres in the spinning industry, circular metallic containers called cans, with closed coil helical compression springs inside, are used for laying down the fibre strand [1–2]. These cans are transported and used to feed the material from one machine to another in the process sequence. The closed coil helical compression spring is an imperative element of a can

Corresponding author/*Korespondenčni avtor:*
Sukhvir Singh
E-mail: sukh7911@gmail.com

used for a uniform deposition and withdrawal of sliver to avoid any undue stretching of sliver, which is very weak. Combed cotton drafted sliver is a rope-like structure and most of the fibres are oriented parallel to the sliver axis. Due to very low inter-fibre cohesion, the combed sliver is susceptible to undesirable stretching at the time of sliver deposition at the draw-frame and during sliver withdrawal in subsequent machine processes.

The can-springs used for sliver storage are subjected to repeated reversals of loading over a prolonged period of time resulting in their degradation due to fatigue; consequently, with the passage of time, their stiffness reduces [3–4]. Therefore, an older can-spring will deflect more in comparison to a newer one made of the same material, against the same applied load. In the case of low can-spring stiffness, there are chances of sliver stretching due to its own weight in the unsupported region, as shown in Figure 1. (L + L1) is the sliver length contributing in sliver stretching during processing. In consequence, the combed sliver, roving and resultant combed yarn quality characteristics are found significantly influenced [5–8]. The optimum storage can-spring pressure should be maintained for smoother operations [9].

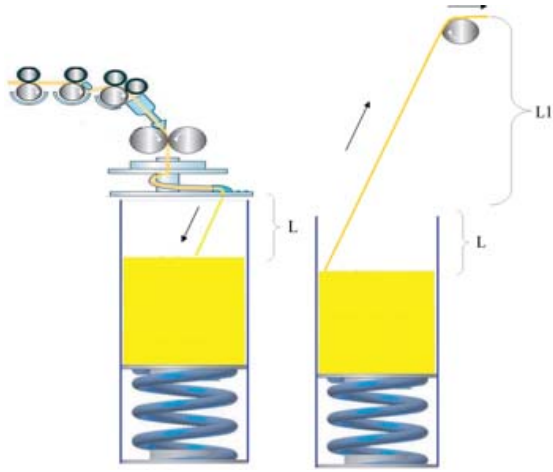

a) Silver deposition at the delivery section

b) Silver with drawal at speed-frame creel

Figure 1: Combed sliver deposition and withdrawal from older storage can: a) sliver deposition at delivery section; b) sliver withdrawal at speed-frame creel

The non-uniform deformation of a can-spring may severely influence sliver quality at the time of deposition and withdrawal of sliver on subsequent machine passages. Modelling the dynamics of the can-spring sliver deposition/withdrawal system is necessary to develop the understanding of the system and to study the effects of variation of can-spring stiffness, rate of deposition and withdrawal of sliver, etc. on the quality of sliver and yarn. The variation of mass on the top plate due to the deposition or withdrawal of sliver makes the task of developing the model relatively challenging. A review of the literature reveals that modelling such a system with variation in its inertia has not been carried out yet.

2 Materials and methods

Combed cotton sliver of 14.22 ktex produced from an extra-long variety MCU-5 from the south Indian states was used for this study. A bond graph model for the can-spring sliver deposition/withdrawal system was developed systematically from first principles. The model explains the transactions of power and understanding of the *cause-effect* relationships between the interacting subsystems. The model facilitates the study of the effect of sliver can-spring stiffness and the rate of sliver deposition or withdrawal on the forces experienced by the combed sliver and top plate through simulations and analysis.

2.1 Brief introduction of bond graph technique

A bond graph is a unified approach to the modelling of physical system dynamics. The bond graph approach was originally developed and presented by H. M. Paynter at MIT in 1959. Bond graph is a pictorial or graphical representation of the dynamics of a physical system based on power transactions between component elements and subsystems [10–12]. The cause and effect relationships, or *causality*, are represented elegantly through the *causal strokes* on the bonds. The bond graph approach has numerous advantages over conventional simulation. It provides a graphical representation of the model of dynamics and systematic extraction of system equations algorithmically [11].

In a physical system, only the exchange and conversion of energy in different forms take place. Power (P) is the change in energy (E) with respect to time (t) and can be expressed as:

$$P = \frac{dE}{dt} \quad (1).$$

The power transacted using bonds through the parts of a bond graph can be expressed as the product of effort (e) and flow (f) variables which are functions of time (t):

$$P = e(t) \cdot f(t) \quad (2).$$

2.2 System elements used in bond graph modelling approach

The bond graph elements are categorised as *Sources* (or active elements), *Passive elements*, *Converters* and *Junctions* [10].

2.2.1 Source elements

In the bond graph approach, there are two kinds of source elements, i.e. a source of effort and a source of flow. The source of effort (S_e) imposes an effort on the system irrespective of the flow in return which is decided by the system, as shown in Figure 2a. In the same way, the source of flow (S_f) imposes a flow on the system irrespective of the returning effort which is decided by the system, as shown in Figure 2b. The cause and effect relationship in terms of causality remains fixed for source elements, as shown below in Figure 2. For a power bond connecting two subsystems, if effort is decided by the subsystem at one end, the flow will be decided by the subsystem at the other end. Both the effort and flow associated with a bond cannot be determined by the system at any end. The assignment of causality is an algorithmic process. In a bond graph representation, a causal stroke is placed on the bond at the effort receiving end. The other end of the bond automatically receives the flow.

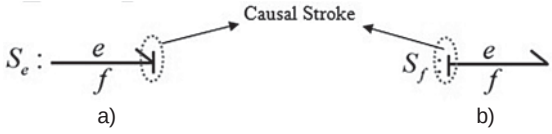

Figure 2: Source elements: a) source of effort; b) source of flow

2.2.2 Junction elements

There are two junction elements which connect different parts in a bond graph. These are the 0-junction and 1-junction. The 0-junction is an effort equalising junction; thus, efforts in all the bonds connected to it remain the same, as depicted in Figure 3a. The flow relationship can be expressed as given below:

$$f_1 = f_2 + f_3 + f_4 \quad (3).$$

In the case of the 1-junction, the flow remains the same in all the bonds connected to it. It acts as a flow equalising junction, as shown in Figure 3b. The efforts summing at this junction can be expressed with equation 4:

$$e_1 = e_2 + e_3 + e_4 \quad (4).$$

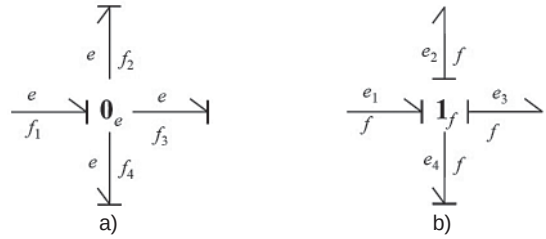

Figure 3: Junction elements: a) 0-junction; b) 1-junction

2.2.3 Compliance element

In natural or integral causality, the C-element receives the flow from the system and gives back effort to the system, as shown in Figure 4. The variable q associated with the C-element is the generalised displacement. K represents the stiffness associated with it.

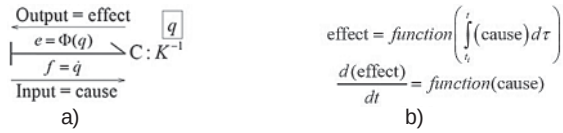

Figure 4: Compliance element: a) representation of output and input; 4b) cause and effect relationship for integrally causalled C-element

The output of the C-element is effort, which is a function of its state variable q, given as:

$$e_{(t)} = \Phi(q) = K \cdot q = K\int_{t_1}^{t} \dot{q} d\tau = K\int_{t_1}^{t} f(\tau) d\tau \quad (5).$$

2.2.4 Inertia element

In its natural or integral causality, the I-element receives effort from the system and gives back the flow to the system, as shown in Figure 5. The state variable

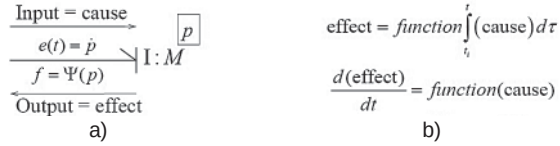

Figure 5: Inertia element: a) representation of output and input; b) cause and effect relationship of I-element

associated with the I-element is the generalised momentum p. M is the mass associated with the I-element.

The output of the I-element is flow, which is a function of its state variable p:

$$f_{(t)} = \Psi(p) = \frac{P}{M} = \frac{1}{M}\int_{t_1}^{t} \dot{p}\,d\tau = \frac{1}{M}\int_{t_1}^{t} e(\tau)\,d\tau \qquad (6).$$

2.2.5 Resistive element

The R-element is used to represent dissipation. It can be causalled in both ways, depending on the invertibility exhibited by the phenomenon. The two types of causality in the case of the R-element are shown in Figure 6.

$$f = \frac{e}{R} = \Phi(e)$$

$$e = R \cdot f = \Phi(f)$$

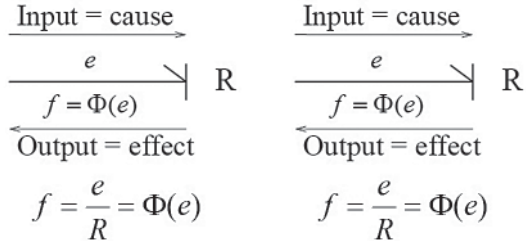

Figure 6: Causality for R-element

2.2.6 Transformer element

TF represents the transformer element in a bond graph. It can relate an input flow to the output flow, and an input effort to the output effort, as shown in Figure 7. This flow to flow or effort to effort relationship is established through the transformation modulus μ.

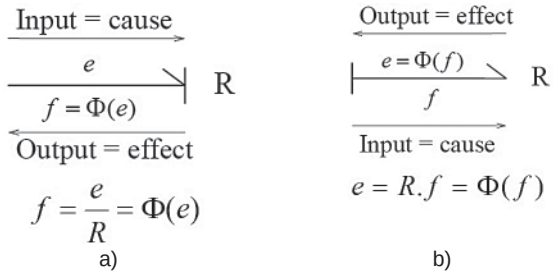

Figure 7: Flow to flow and effort to effort relationship at transformer

2.2.7 Gyrator element

The GY-element represents the gyrator in a bond graph. It relates the input flow to the output effort, and vice-versa. This flow to effort and effort to flow relationship is established using the modulus μ, as shown in Figure 8.

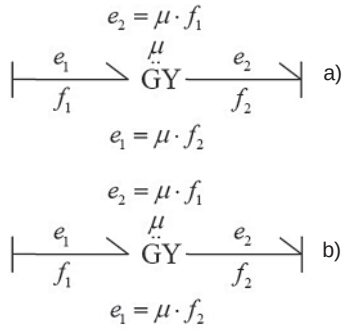

Figure 8: Flow to effort and effort to flow relationship represented by gyrator

Using the power bond and the nine elements of the bond graph, the dynamics of the physical system in any energy domain or a combination of energy domains can be modelled.

2.3 Theoretical modelling of can-spring mechanism using bond graph

An attempt was made to study the dynamics of the can-spring mechanism used at the finisher draw-frame stage for sliver storage. It was presumed that the combed cotton sliver deposited over the top plate has uniform linear density or fineness and that the weight of sliver deposited per second over the top plate remains constant. For an accurate prediction of the can-spring mechanism, real values of independent variables based on industrial experience were considered for evaluation. Also, an in-depth study of sliver quality characteristics was conducted while selecting sliver linear density, inter-fibre cohesion and lengthwise sliver uniformity. The schematic diagram of the can-spring mechanism is shown in Figure 9.

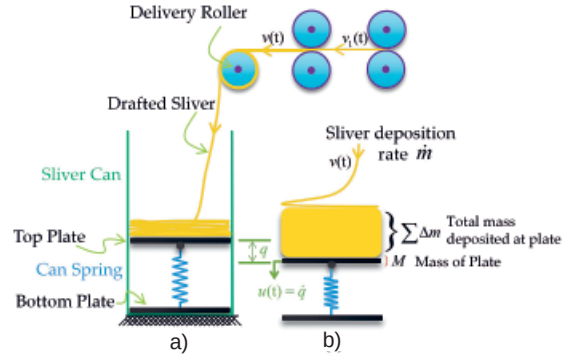

Figure 9: (a) Sliver storage at draw-frame delivery, (b) can-spring mechanisms at draw-frame

The following nomenclature was adopted:
M = initial mass of the top plate before sliver deposition takes place.
Δm = increment in mass of deposited sliver on the top plate in the time duration Δt.
u = velocity of the top plate at time t.
v = flow velocity of sliver at time t, before depositing on the top plate.
$q(t)$ = deformation in can-spring due to applied load of deposited sliver at time t.
g = acceleration due to gravity
$(\Sigma\Delta m + \Delta m)$ = total weight on the top plate at an instance due to small increment of combed sliver weight.

The linear momentum of the top plate, along with deposited sliver on it at time t can be expressed as

$$p(t) = M \cdot u(t) + (\Sigma\Delta m) \cdot u(t) + \Delta m \cdot v(t) \quad (7).$$

Considering that the deposited sliver moves with the same velocity as that of the top plate, after the sliver deposition $(u + \Delta u)$ is equivalent to $(v + \Delta v)$. The flow velocity of sliver $v(t)$ is equal to $u(t)$ after the sliver deposition and will follow the velocity of the top plate. The linear momentum of the top plate at time $(t + \Delta t)$ can be expressed as

$$p(t + \Delta t) = M \cdot (u + \Delta u) + (\Sigma\Delta m) \cdot (u + \Delta u) + \\ + \Delta m \cdot (u + \Delta u) \quad (8).$$

On subtracting equation (7) from equation (8), and on dividing both sides by Δt, we get

$$\lim_{\Delta t \to 0}\left(\frac{p(t+\Delta t) - p(t)}{\Delta t}\right) = \lim_{\Delta t \to 0}\left(M\,\frac{\Delta u}{\Delta t} + (\Sigma\Delta m)\,\frac{\Delta u}{\Delta t} + \right. \\ \left. + \frac{\Delta m \Delta u}{\Delta t}\right) + \frac{\Delta m}{\Delta t}\,u(t) - \frac{\Delta m}{\Delta t}\,v(t) \quad (9),$$

$$\therefore \lim_{\Delta t \to 0}\left(\frac{\Delta m \Delta u}{\Delta t}\right) = 0,$$

$$\frac{dp}{dt} = M\frac{du}{dt} + \lim_{\Delta t \to 0}\left(\frac{(\Sigma\Delta m)\cdot\Delta u}{\Delta t}\cdot\left(\frac{\Delta t}{\Delta t}\right)\right) - \\ - \dot{m}v(t) + \dot{m}u(t) \quad (10),$$

$$\frac{dp}{dt} = M\frac{du}{dt} + \left(\int^{t}\frac{dm}{d\tau}\,d\tau\right)\cdot\frac{du}{dt} - \dot{m}v(t) + \dot{m}u(t) \quad (11),$$

$$\frac{dp}{dt} = \frac{d}{dt}\left[(M + \int^{t}\dot{m}\cdot \mathrm{d}\tau)\cdot u\right] - \dot{m}v(t) \quad (12).$$

The rate of change of the linear momentum of the top plate is caused by the forces acting on it and can also be expressed as given in (13)

$$\frac{dp}{dt} = -\left[M + \frac{(\Sigma\Delta m + \Delta m)\cdot\Delta t}{\Delta t}\right]\cdot g - F_K(q) - F_R(u) \quad (13),$$

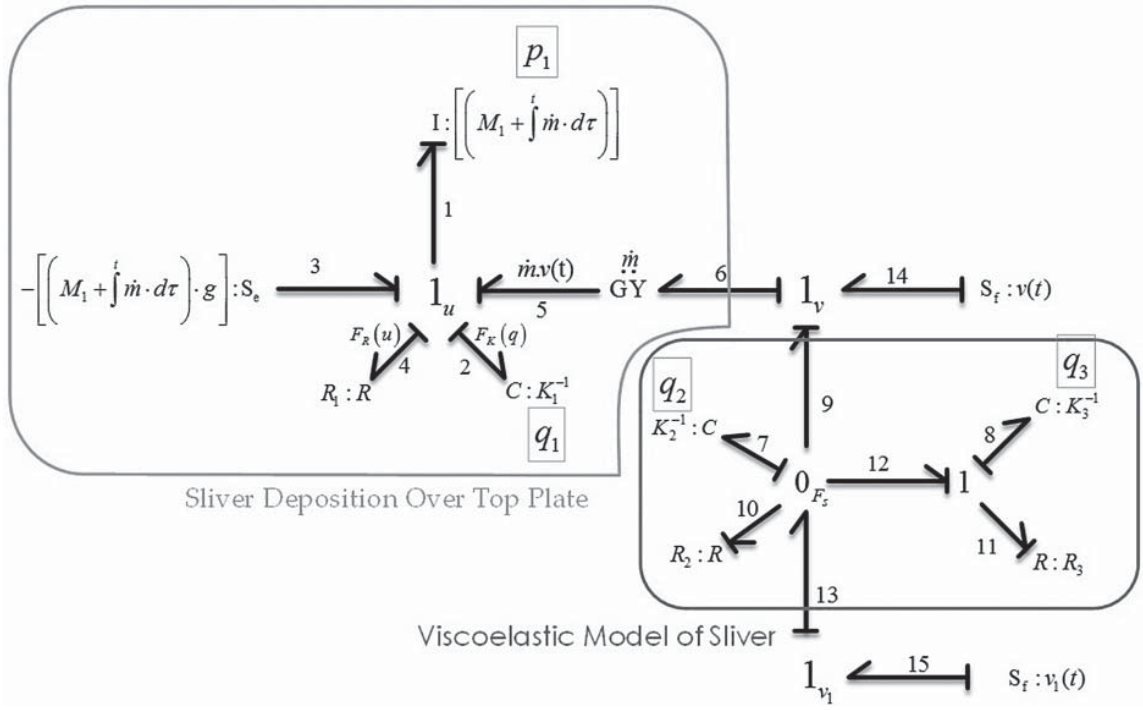

Figure 10: Bond graph model of sliver deposition at draw-frame delivery

where

$$F_K = K \cdot q(t) \tag{14}$$

and

$$F_R = \dot{m} \cdot \dot{q} = \dot{m} \cdot u(t) \tag{15},$$

$$\frac{dp}{dt} = -\left[M + \int^{t} \frac{dm}{d\tau} \cdot d\tau\right] \cdot g - F_K(q) - F_R(u) \tag{16}.$$

By comparing (16) with (12),

$$\frac{d}{dt} = [(M + \int^{t} \dot{m} \cdot d\tau) \cdot u] =$$
$$= -\ [M + \int^{t} \dot{m} \cdot \mathrm{d}\tau] \cdot g - F_K(q) - F_R(u) + \dot{m}v(t) \tag{17}.$$

This represents the formulation of dynamics for the can-spring system.
Equation (17) is represented graphically as outlined in green in the bond graph of Figure 10.

2.4 Viscoelastic representation of sliver

For the purpose of modelling, the Kelvin-Voigt model, the Maxwell model and the standard model were studied initially. The standard model consists of two springs and a dashpot. It is the simplest model that describes both creep and stress relation behaviour of a viscoelastic material. Based on the observed behaviour of the combed sliver, the widely accepted Kelvin representation of the standard model was used. A minor modification was made in the Kelvin representation of the standard model by considering a permanent deformation due to R_2 in the viscous region which appears to be a more suitable representation of the viscoelastic nature of combed sliver, as shown in Figure 11. This viscoelastic behaviour was already modelled in the bond graph of Figure 10.

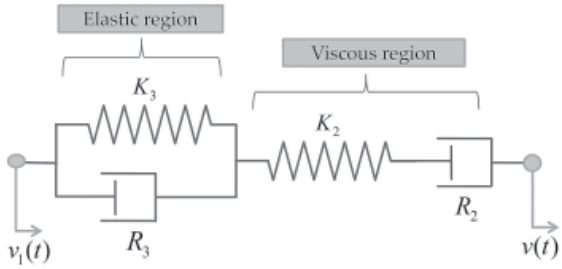

Figure 11: Representation of viscoelastic behaviour of sliver

2.5 Deriving system equations from bond graph

System equations can be derived algorithmically from the bond graph model as a set of the first order differential equations, using the following two equations:
What do the elements give to the system?

$$Se = e_3 = -[(M_1 + \int^{t} \dot{m} \cdot dt)] \tag{18}$$

$$f_1 = \frac{p_1}{(M_1 + \int^{t} \dot{m} \cdot dt)} \therefore f_1 = f_3 = f_4 = f_2 = f_5 \tag{19}$$

$$e_4 = R_1 \cdot f_4 = R_1 \cdot \frac{p_1}{(M_1 + \int^{t} \dot{m} \cdot dt)} \tag{20}$$

$$e_2 = K_1 \cdot q_1 \tag{21}$$

$$S_{f_{14}} = f_{14} = v(t) \tag{22}$$

$$S_{f_{15}} = f_{15} = v_1(t) \tag{23}$$

$$e_8 = K_3 \cdot q_3 \tag{24}$$

$$e_7 = K_2 \cdot q_2 \therefore e_7 = e_9 = e_{10} = e_{13} = e_{12} \tag{25}$$

$$f_{11} = \frac{e_{11}}{R_3} = \frac{e_{12} - e_8}{R_3} = \frac{K_2 \cdot q_2 - K_3 \cdot q_3}{R_3} \tag{26}$$

$$f_{10} = \frac{K_2 \cdot q_2}{R_2} \tag{27}$$

$$e_5 = \dot{m} \cdot f_6 = \dot{m} \cdot f_{14} = \dot{m} \cdot v(t) \tag{28}$$

$$e_6 = \dot{m} \cdot f_5 = \dot{m} \cdot f_1 = \dot{m} \cdot \frac{p_1}{(M_1 + \int^{t} \dot{m} \cdot dt)} \tag{29}$$

What do the integrally causalled storage elements receive from the system?

$$\dot{p_1} = e_1 = e_3 + e_5 - e_2 - e_4 \tag{30}$$

$$\dot{p_1} = -(M_1 + \int^{t} \dot{m} \cdot dt) \cdot g + \dot{m} \cdot v(t) -$$
$$- K_1 \cdot q_1 - R_1 \cdot \frac{p_1}{(M_1 + \int^{t} \dot{m} \cdot dt)} \tag{31}$$

$$\dot{q_1} = f_2 = f_1 = \frac{p_1}{[(M_1 + \int^{t} \dot{m} \cdot dt)]} \tag{32}$$

$$\dot{q_3} = f_8 = f_{12} = f_{11} = f_{11} =$$
$$= \frac{e_{11}}{R_3} = \frac{e_{12} - e_8}{R_3} = \frac{K_2 \cdot q_2 - K_3 \cdot q_3}{R_3} \tag{33}$$

$$\dot{q}_2 = f_7 = f_{13} - f_9 - f_{12} - f_{10} \quad (34)$$

$$\dot{q}_2 = f_7 = f_{13} - f_9 - f_{12} - f_{10} = f_{15} - f_{14} - f_{11} - f_{10} \quad (35)$$

$$\dot{q}_2 = v_1(t) - v(t) = \frac{K_2 \cdot q_2 - K_3 \cdot q_3}{R_3} - \frac{K_2 \cdot q_2}{R_2} \quad (36)$$

The first order equations obtained from the bond graph model can be conveniently simulated numerically using solvers for ordinary differential equations provided by any of the available computational programming software such as Matlab, Scilab etc.

3 Results and discussion

In order to study the simulated behaviour of the can-spring mechanism, some initial conditions were presumed considering the realistic values of parameters during sliver storage and are mentioned in Table 1.

The linear momentum and displacement of the top plate built up with time and direction was considered as negative. This was due to the energy build up in the storage spring through compression, as shown in Figure 12. Similarly, it was observed that after a sudden initial impact of the sliver on the top plate, the velocity of the top plate remained almost constant with a small decrease over time. Furthermore, the mass deposited over the top plate increased with time depending on the sliver deposition rate, as shown in Figure 12.

Table 1: Initial conditions/input data used in simulation

Parameter	Unit	Value
Initial mass of top plate (M)	kg	0.250
Can-spring stiffness (K)	N/m	163.3
Flow velocity of sliver at time (t)	m/s	5
Acceleration due to gravity (g)	m/s^2	9.81
Rate of change of mass over top plate ($\dot{m}$)	kg/s	0.0255
Time span (s)	s	750

Linear stretching remained due to the viscoelastic part of the model q_7 almost unchanged with the passage of time, and the sliver deformation in the elastic region q_8 experienced a sudden increase within a short time. After that, it remained constant, as shown in Figure 13. Moreover, the force experienced by the can-spring increased with an increase in its deformation, as shown in Figure 14. The latter agrees with the deformation of the can-spring as

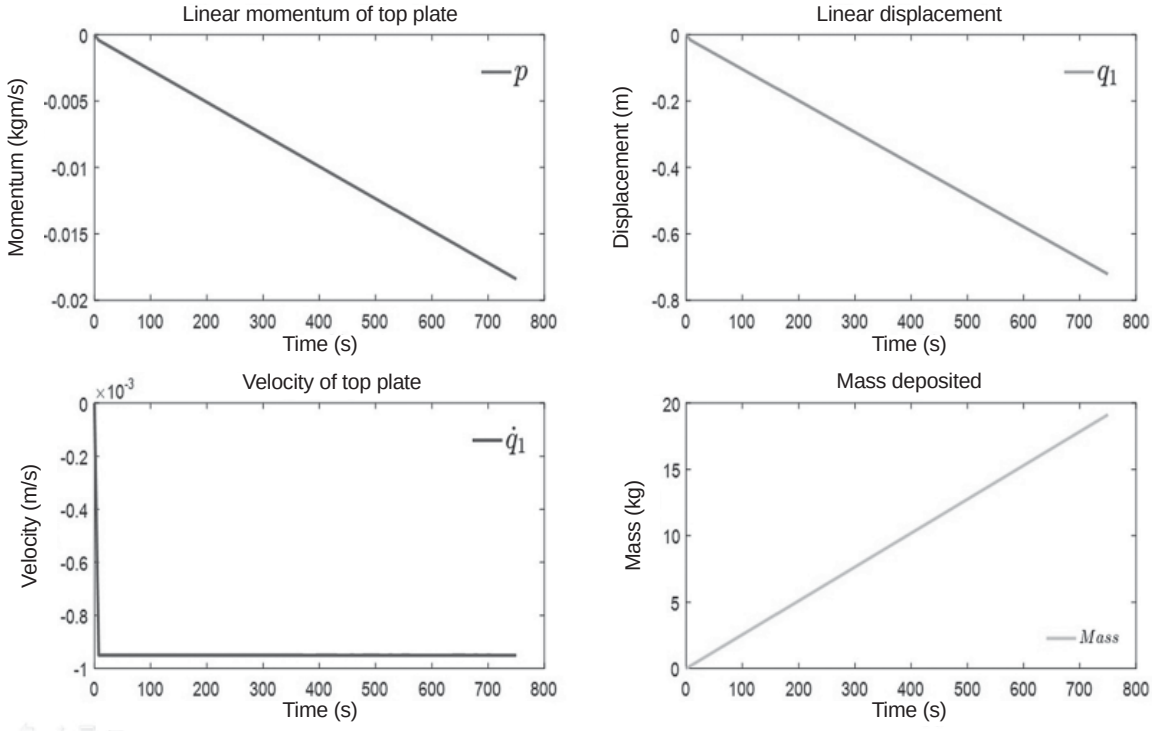

Figure 12: Linear momentum, displacement, velocity and mass responses with time

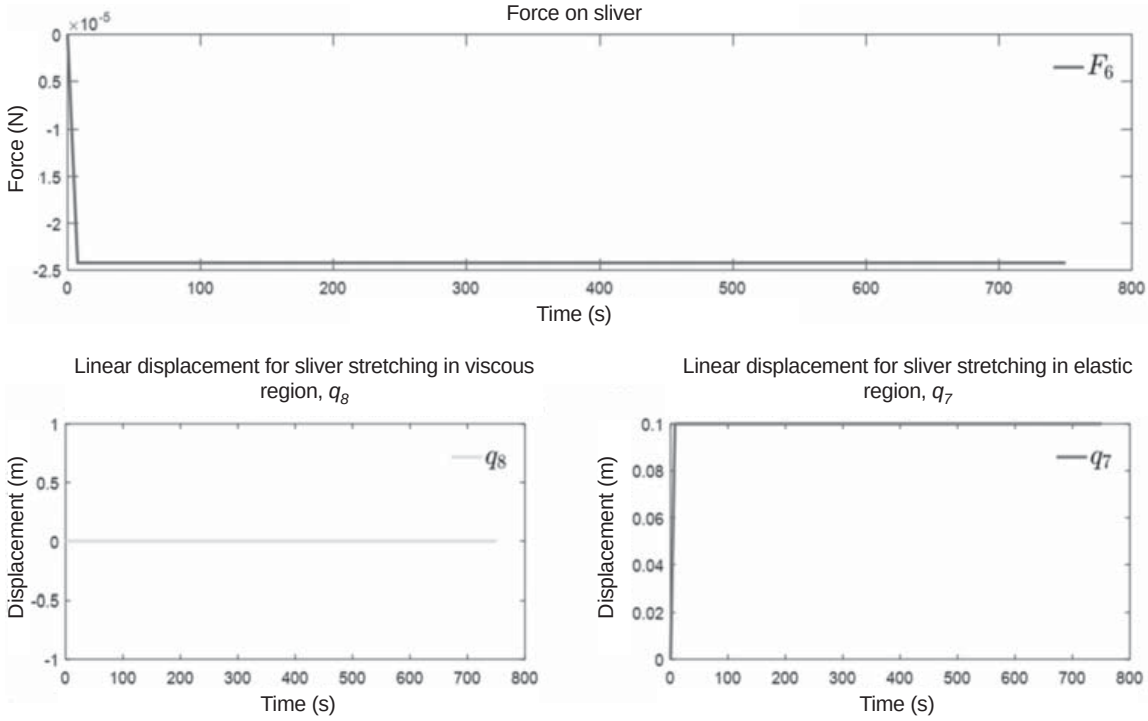

Figure 13: Force on sliver and sliver stretching in viscoelastic region with time

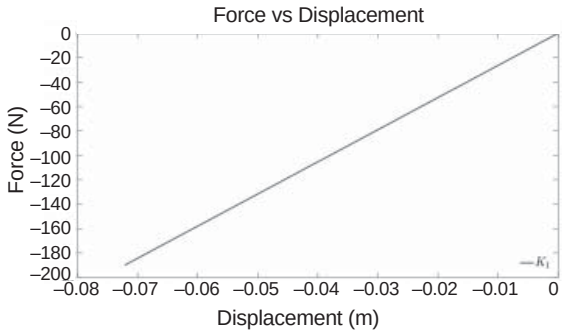

Figure 14: Force experienced by storage spring versus displacement

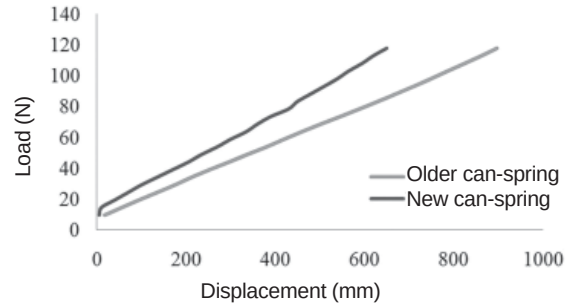

Figure 15: Load versus displacement curve for new and older can-spring

observed from the experimental work shown in Figure 15. It is found that the force on the can-spring built up in the negative direction due to compression of the can-spring since the deposited sliver mass increased with time, as shown in Figure 14. In the case of sliver withdrawal from storage cans, the force experienced by the can-spring gradually reduced due to the decrease in the amount of sliver mass over the top plate with time during sliver withdrawn, as shown in Figure 15.

4 Conclusion

In order to study the dynamics of the can-spring mechanism, a bond graph model was developed. It was established that sliver deformation in the elastic region q_8 experienced a sudden increase within a short time and after that remained constant whereas q_7 remained unchanged. The mass deposited over the top plate increased with the increase in time. It was found out that the linear momentum of the top

plate and its displacement increased with time. The velocity of the top plate showed a peak in short time initially during sliver deposition and remained unchanged afterwards. The force experienced by the storage can-spring also built up as a result of the can-spring compression due to the increase in the deposited sliver mass with time. The force experienced by the sliver showed an initial sudden increment followed by a downfall and then remained unchanged. It can be inferred that a small undesirable deflection can deteriorate the sliver structure and can alter the sliver configuration during drafting operation. It was found that the linear momentum of the top plate increased in the negative direction over time depending on sliver linear density and sliver deposition rate. However, a more rigorous study is required to study the accurate dynamics of such precise systems as the force and stresses experienced by the sliver are too low due to very low inter-fibre cohesion. The current bond graph model can be used for a further investigation for a more accurate prediction based on the dynamics of the can-spring-sliver system behaviour used for combed sliver handling.

References

1. ARORA, V., SINHA, S. K. Sliver cans – an influencing factor of yarn quality. *Textile Trends*, 1998, **41**, 27–30.
2. RIMTEX Sliver handling systems [online]. RIMTEX Industries [accessed 27 .2. 2020]. Available on World Wide Web: <https://www.rimtex.com/>.
3. UGURAL, Ansel C. *Mechanical design of machine components*. 2nd ed. Boca Raton, New York, London : CRC Press, Taylor & Francis, 2016, 652–683.
4. CHESLEY, James C. *Handbook of reliability prediction procedures for mechanical equipment*. West Bethesda, Maryland : NSWC Carderock Division, 2011, 4.1–4.41.
5. SINGH, Sukhvir, BHOWMICK, Niranjan, VAZ, Anand. Effect of finisher draw frame variables on combed cotton yarn quality. *Tekstilec,* 2018, **61**(4), 245–253, doi: 10.14502/Tekstilec2018.61.245–253.
6. SINGH, Sukhvir, BHOWMICK, Niranjan and VAZ, Anand. Influence of can-spring stiffness, deliver rate and sliver coils position on unevenness. *Journal of Textile and Apparel, Technology and Management*, 2019, **11**(1), 1–12.
7. SINGH, Sukhvir, BHOWMICK, Niranjan, VAZ, Anand. Effect of can-storage parameters of finisher draw-frame on combed ring-spun yarn quality. *Research Journal of Textile and Apparel,* 2019, **23**(2), 153–167, doi: 10.1108/RJTA-06-2018-0040.
8. SINGH, Sukhvir, BHOWMICK, Niranjan, VAZ, Anand. Impact of finisher draw-frame storage variables on combed yarn quality. *Tekstilec*, 2019, **62**(2), 110–123, doi: 10.14502/Tekstilec2019.62.110-123.
9. GHOSH, A., MAJUMDAR, A. Process control in drawing, combing and speedframe operations. In *Process Control in Textile Manufacturing*. 1st ed. Edited by V. Kothari, R. Alagirusamy, A. Das and A. Majumdar. New Delhi : Woodhead Publishing, 2013, 158–190.
10. KARNOPP, D. C., MARGOLIS, D. L., ROSENBERG, R. C. *System dynamics, modeling and simulation of mechatronic systems.* New York : John Wiley & Sons, 2000.
11. MUKHERJEE, A., KARMAKAR, R., SAMANTARAY, A. K. *Bond graph in modeling, simulation and fault identification*. 2nd ed. Boca Raton : CRC Press, 2006.
12. BORUTZKY, W. *Bond graphs : a methodology for modelling multidisciplinary dynamic systems*. San Diego : SCS Publishing House, 2004.